Inorganic Chemistry

Article

pubs.acs.org/IC

Ferromagnetic Dinuclear Mixed-Valence Mn(II)/Mn(III) Complexes: Building Blocks for the Higher Nuclearity Complexes. Structure, Magnetic Properties, and Density Functional Theory Calculations

Mikko M. Hänninen,[†] Juha Välivaara,[†] Antonio J. Mota,[‡] Enrique Colacio,*[,‡] Francesc Lloret,[§] and Reijo Sillanpää*[,†]

[†]Department of Chemistry, University of Jyväskylä, P.O. Box 35, 40014 Jyväskylä, Finland

[‡]Departamento de Química Inorgánica, Facultad de Ciencias, Universidad de Granada, Avda. Fuentenueva s/n, 18002 Granada, Spain

[§]Instituto de Ciencia Molecular (ICMOL), Universitat de València, 46980 Paterna, València, Spain

Supporting Information

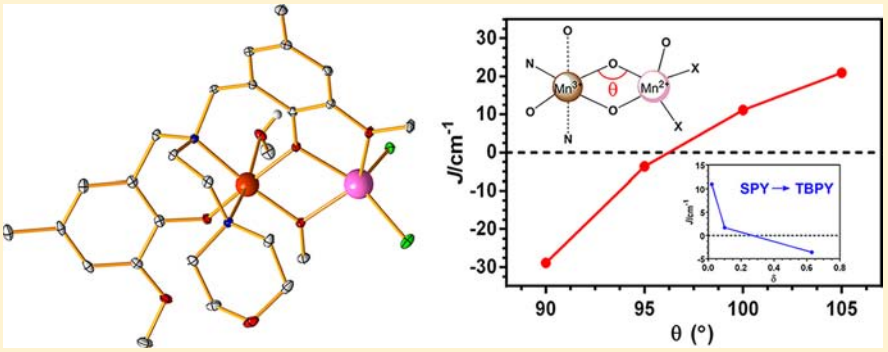

ABSTRACT: A series of six mixed-valence Mn(II)/Mn(III) dinuclear complexes were synthesized and characterized by X-ray diffraction. The reactivity of the complexes was surveyed, and structures of three additional trinuclear mixed-valence Mn(III)/Mn(II)/Mn(III) species were resolved. The magnetic properties of the complexes were studied in detail both experimentally and theoretically. All dinuclear complexes show ferromagnetic intramolecular interactions, which were justified on the basis of the electronic structures of the Mn(II) and Mn(III) ions. The large Mn(II)−O−Mn(III) bond angle and small distortion of the Mn(II) cation from the ideal square pyramidal geometry were shown to enhance the ferromagnetic interactions since these geometrical conditions seem to favor the orthogonal arrangement of the magnetic orbitals.

INTRODUCTION

Polynuclear manganese complexes have been profusely studied for many years due to their relevance in fields such as metalloenzymes and molecular magnetism. As far the former field is concerned, it should be pointed out that many biological processes are catalyzed by di- and tetramanganese enzymes. These include catalases (hydrogen peroxide disproportionation),[1−3] arginase (L-arginine hydrolysis),[4] sulfur-oxidizing enzyme (energy metabolism in thiobacilli),[5] xylose isomerase (isomerization of, e.g., glucose to fructose),[6−8] hydrolases (phosphodiester, -triester and phosphoamide hydrolysis), class Ib ribonucleotide reductase,[9] and water oxidase (photosynthetic oxygen production).[10] The work in this area has been focused on the preparation of polynuclear manganese model compounds, including mixed-valence complexes, to mimic the structure, physical properties, and function of the active center of the metalloenzyme with the ultimate goal of elucidating its mechanism of action.

With regard to the field of molecular magnetism, it has undergone a renaissance with the discovery two decades ago of the paradigmatic complex Mn12Ac, containing Mn(IV) and anisotropic Mn(III) centers connected by oxo-bridging ligands, exhibiting slow relaxation of the magnetization and magnetic hysteresis below the so-called blocking temperature (T_B) without undergoing three-dimensional (3D) magnetic ordering.[11] From that moment onward numerous metal complexes exhibiting slow relaxation of the magnetization were prepared, mainly being Mn clusters containing at least some Mn^{III} centers. These nanomagnets, called single-molecule magnets (SMMs),[12] straddle the quantum/classical interface showing quantum effects such as quantum tunnelling of the magnetization and quantum phase interference. They are also potential candidates for magnetic information storage and quantum computing.[13] The origin of the SMM behavior is the existence of an energy barrier (Δ) that prevents reversal of the molecular magnetization and causes slow relaxation of the magnetization at low temperature. This energy barrier depends on the large-spin multiplicity of the ground state (S_T) and the easy-axis (or Ising-type) magnetic anisotropy of the entire molecule ($D < 0$).

Received: December 12, 2012
Published: January 30, 2013

   dx.doi.org/10.1021/ic302731z | Inorg. Chem. 2013, 52, 2228−2241

Proceeding from serendipitous synthesis[14] to a more rational design of these complexes (with potential SMM behavior) we have to be able to control the nuclearity and the bridging atoms and/or molecules to produce compounds with desired properties. This is not a straightforward task, especially when the syntheses begin with a large amount of smaller building blocks. One solution to this problem is a stepwise synthesis of the SMMs which can be done by synthesizing complexes with only few *ferromagnetically coupled* metal ions and potential *reactive sites* which can be utilized in follow-up reactions to increase the nuclearity (and thus total spin) of the compounds.[15] By carefully choosing the reactive components, these reactions could be furthermore used to acquire the appropriate symmetry for the product.[16]

To apply this strategy in practice, we have prepared novel compartmental aminobis(phenolate) ligands which can have up to seven donor atoms (five oxygens and two nitrogens) and several different coordination modes for one or more metal ions (Figure 1). In these ligands the donor atoms are

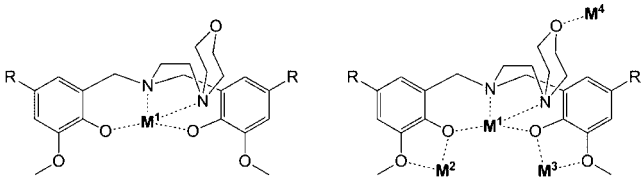

Figure 1. Two examples of the possible coordination modes of aminobis(phenolate)-based ligands.

positioned around the whole molecule. Thus, they can act also as hydrogen bond acceptors and direct the crystallization process when they are not coordinated to metal ions. This family of aminobis(phenolate) ligands was made to react with Mn^{2+} in basic conditions under air to obtain mixed-valence $Mn^{II}Mn^{III}$ complexes. It should be noted that only a few examples of magnetically and structurally characterized mixed-valence $Mn^{II}Mn^{III}$ complexes have been reported so far, which can exhibit either weak ferro- or antiferromagnetic interactions between the Mn^{II} and Mn^{III} metal ions.

In this study, we report the syntheses, reactivity, and magnetic behavior of six new phenoxo-alkoxo heterobridged mixed-valence $Mn^{II}Mn^{III}$ dinuclear complexes of general formula $[Mn^{II}Mn^{III}(\mu\text{-}L)(\mu\text{-}OR)Cl_2D]$ (R = Me or Et and D = MeOH or EtOH). In addition, we have surveyed the reactivity of the dinuclear complexes with either different anions (acetate and nitrate) or ethylene glycol giving rise to three novel $Mn^{II}Mn^{III}Mn^{II}$ trinuclear complexes. The aim of this work is 2-fold: (i) to disclose how the structural factors of the bridging network affect the magnetic exchange interaction in this type of mixed-valence $Mn^{II}Mn^{III}$ complexes, which would allow the rational preparation of $Mn^{II}Mn^{III}$ complexes with ferromagnetic exchange interaction, and (ii) to figure out if the $Mn^{II}Mn^{III}$ complexes containing highly anisotropic Mn^{III} ions and ferromagnetic coupling between metal ions leading to a high spin ground state that can exhibit SMM behavior.

EXPERIMENTAL SECTION

General Procedures. All starting materials were reagent grade, purchased from Sigma Aldrich and used as received. Solvents were HPLC grade and used without any additional drying. All syntheses were performed under ambient laboratory atmosphere. Elemental analysis was performed by using a Vario El III elemental analyzer. Single-crystal X-ray measurements were performed by using either Enraf Nonius Kappa CCD area detector diffractometer with the use of graphite monochromated Mo-Kα radiation or with Agilent SuperNova dual wavelength diffractometer equipped with Atlas CCD area detector using Cu−Kα radiation. Variable-temperature (2−300 K) magnetic susceptibility measurements on polycrystalline samples were carried out with a Quantum Design Squid MPMSXL-5 device operating at 1 T from room temperature to 50 K and at 0.05 T from this latter temperature to 2 K. The experimental susceptibilities were corrected for the diamagnetism of the constituent atoms by using Pascal's tables. Reflectance diffuse spectra were recorded with a Varian Cary 5E UV−vis-NIR spectrophotometer and the XPS spectra with a Kratos AXIS Ultra spectrophotometer.

Ligand Syntheses. Ligands H_2L1 and H_2L2 were synthesized using our recently published thermal oven method[23] following the general procedure. Phenol (eugenol or 2-methoxy-4-methylphenol), paraformaldehyde, and 4-(2-aminoethyl)morpholine were weighed into a 25 mL beaker which was placed inside a 100 mL beaker and covered with a watch glass. This reaction container was placed in thermal oven at 120 °C for 1.5 h. The formed yellow oil was dissolved in ethanol (H_2L1) or ethanol−water mixture (H_2L2) and was left to crystallize for a few days. The white (slightly yellowish for H_2L2) precipitate was filtered and air-dried to get synthesis-pure products with good yields. For ^1H NMR and elemental analysis of the ligands, see Supporting Information.

Complex Syntheses. Complex **1** was synthesized by dissolving 1.0 mmol (198 mg) of $MnCl_2{\cdot}6H_2O$ into 15 mL of methanol and 0.5 mmol (242 mg) of H_2L1 was added to the solution. Then, 1.0 mmol (140 μL) of triethylamine was added to neutralize the formed hydrochloric acid, and the mixture was heated at 65 °C for 45 min. After the solution had cooled to room temperature, the formed dark green precipitate was separated by filtration. X-ray diffraction quality crystals were grown in six days by placing solutions with the above-mentioned molar amounts into a fridge without preheating the solution. Yield: 241 mg (66%). Elemental analysis: $C_{30}H_{43}Cl_2Mn_2N_2O_7$ (724.45): calcd. C 49.74, H 5.98, N 3.87; found C 49.50, H 6.03, N 3.91.

Complex **2** was synthesized by dissolving 0.6 mmol (119 mg) of $MnCl_2{\cdot}6H_2O$ into 15 mL of methanol, and 0.5 mmol (130 mg) of H_2L2 was added to the solution. Then, 0.6 mmol (84 μL) of triethylamine was added to neutralize the formed hydrochloric acid, and the mixture was heated at 65 °C for 30 min. After the solution had cooled to room temperature, the solution was concentrated to ca. 10 mL by rotary evaporator. X-ray diffraction quality crystals were formed in two days and were separated by filtration. Yield: 138 mg (69%). Elemental analysis: $C_{26}H_{41}Cl_2Mn_2N_2O_7$ (672.38): calcd. C 46.44, H 5.85, N 4.17; found C 46.40, H 5.91, N 4.05.

Complex **3** was synthesized by dissolving 0.5 mmol (99 mg) of $MnCl_2{\cdot}6H_2O$ into 13 mL of ethanol, and 0.25 mmol (121 mg) of H_2L1 was added to the solution. Then, 0.5 mmol (70 μL) of triethylamine was added to neutralize the formed hydrochloric acid and the mixture was refluxed for 5 h. After the solution had cooled to room temperature, a dark green precipitate formed and was separated by filtration. X-ray diffraction quality crystals were grown from the solution with the above-mentioned molar amounts at room temperature without heating the solution at any point. Yield: 138 mg (69%). Elemental analysis: $C_{32}H_{47}Cl_2Mn_2N_2O_7$(752.51): calcd. C 51.07, H 6.30, N 3.72; found C 50.54, H 6.20, N 3.61.

Complex **4** was synthesized by dissolving 0.5 mmol (99 mg) of $MnCl_2{\cdot}6H_2O$ into 13 mL of ethanol, and 0.25 mmol (108 mg) of H_2L2 was added to the solution. Then, 0.6 mmol (84 μL) of triethylamine was added to neutralize the formed hydrochloric acid. The reaction vessel was placed in ultrasound bath for half an hour and then left to crystallize at room temperature. Dark green X-ray diffraction quality crystals were formed to solution in two days and were separated by filtration. Yield: 124 mg (76%). Elemental analysis: $C_{26}H_{37}Cl_2Mn_2N_2O_6$(654.36): calcd. C 47.72, H 5.70, N 4.28; found C 47.65, H 5.84, N 4.08.

Complex **5** was synthesized by dissolving 0.4 mmol (115 mg) of $MnBr_2{\cdot}4H_2O$ into 10 mL of methanol and 0.2 mmol (97 mg) of H_2L1 was added to the solution. Then, 0.4 mmol (56 μL) of triethylamine was added to neutralize the formed hydrobromic acid and the mixture was heated at 65 °C for 4 h. After the solution had cooled to room

dx.doi.org/10.1021/ic302731z | Inorg. Chem. 2013, 52, 2228−2241

Table 1. Summary of the Crystallographic Data for Complexes 1−10

	1	2	3	4	5	6	7	8	9	10
formula	$C_{30}H_{43}Cl_2Mn_2N_2O_7$	$C_{26}H_{39}Cl_2Mn_2N_2O_7$	$C_{32}H_{53}Cl_2Mn_2N_2O_8$	$C_{52}H_{74}Cl_4Mn_4N_4O_{12}$	$C_{30}H_{43}Br_2Mn_2N_2O_7$	$C_{30}H_{43}Cl_2Mn_2N_2O_7$	$C_{58}H_{78}Mn_3N_6O_{18}$	$C_{62}H_{84}Mn_3N_4O_{16}$	$C_{62}H_{84}Cl_2Mn_3N_6O_{12}$	$C_{52}H_{74}Cl_4Mn_4N_4O_{14}$
M_r	724.44	672.37	798.56	1308.71	813.36	724.44	1312.08	1306.16	1339.06	1340.74
crystal system	monoclinic	monoclinic	orthorhombic	monoclinic	monoclinic	monoclinic	tetragonal	trigonal	monoclinic	monoclinic
space group (no.)	$P2_1/n$ (14)	$P2_1/n$ (14)	$Pbca$ (61)	$P2_1$ (4)	$P2_1/n$ (14)	$P2_1/n$ (14)	$P4_12_12$ (96)	$R\bar{3}$ (148)	Pc (7)	$P2_1$ (4)
a (Å)	15.1289(7)	14.3344(2)	9.1398(2)	10.6590(2)	15.0159(5)	15.1289(7)	20.7551(6)	41.8678(8)	14.3078(4)	10.6283(3)
b (Å)	9.0452(5)	9.3365(2)	18.5958(3)	19.5525(3)	9.7952(2)	9.0452(5)	20.7551(6)	41.8678(8)	12.8507(3)	19.6048(5)
c (Å)	24.9468(7)	23.4569(3)	41.1345(8)	14.3440(3)	23.8794(8)	24.9468(7)	13.6751(4)	18.9506(4)	17.5189(4)	14.2727(3)
α (°)	90	90	90	90	90	90	90	90	90	90
β (°)	99.164(3)	106.860(1)	90	104.629(1)	102.479(1)	99.164(3)	90	90	98.774(2)	103.831(2)
γ (°)	90	90	90	90	90	90	90	120	90	90
V (Å)	3370.2(3)	3103.53(8)	6991.3(2)	2892.52(9)	3425.68(18)	3370.2(3)	5890.9(3)	28768.3(1)	3183.4(2)	2887.71(13)
Z	4	4	8	2	4	4	4	18	2	2
D_c (g cm^{-1})	1.428	1.487	1.430	1.503	1.577	1.428	1.479	1.357	1.397	1.542
μ (mm^{-1})	0.954	1.063	0.922	1.100	3.115	0.954	5.8110[a]	5.317[a]	0.734	9.214[a]
radiation	Mo−Kα	Mo−Kα	Mo−Kα	Mo−Kα	Mo−Kα	Mo−Kα	Cu−Kα	Cu−Kα	Mo−Kα	Cu−Kα
T/K	123(2)	123(2)	123(2)	123(2)	123(2)	123(2)	123(2)	123(2)	123(2)	123(2)
observed reflections	36564	23476	32669	34810	16598	36564	12125	22823	32104	11876
R_{int}	0.0617	0.0444	0.0358	0.0548	0.0703	0.0617	0.0441	0.0413	0.0597	0.0355
parameters	452	362	424	696	396	452	362	808	807	714
R_1[b]	0.0762 (0.0480)[c]	0.0471 (0.0382)[c]	0.0385 (0.0330)[c]	0.0566 (0.0478)[c]	0.1129 (0.0774)[c]	0.0762 (0.0480)[c]	0.0767 (0.0591)[c]	0.0549 (0.0425)[c]	0.0614 (0.0439)[c]	0.0547 (0.0482)[c]
wR_2[d]	0.1035 (0.0931)	0.0783 (0.0741)	0.0786 (0.0758)	0.1123 (0.1078)	0.2143 (0.1884)	0.1035 (0.0931)	0.1413 (0.1274)	0.1115 (0.1038)	0.0889 (0.0812)	0.1221 (0.1189)
largest difference in peak and hole (e Å^{-3})	0.363− −0.353	0.289− −0.286	0.919− −0.381	1.126− −0.349	1.108− −0.927	0.363− −0.353	0.468− −0.482	0.713− −0.581	0.309− −0.321	1.482 − −0.635

[a]Cu-Kα radiation. [b]$R_1 = \Sigma||F_o| - |F_c||/\Sigma|F_o|$. [c]Values in parentheses for reflections with $I > 2\sigma(I)$. [d]$wR_2 = \{\Sigma[w(F_o^2 - F_c^2)^2]/\Sigma[w(F_o^2)^2]\}^{1/2}$ and $w = 1/[\sigma^2(F_o^2) + (aP)^2 + (bP)]$, where $P = (2F_c^2 + F_o^2)/3$.

dx.doi.org/10.1021/ic302731z | Inorg. Chem. 2013, 52, 2228−2241

Scheme 1. Synthetic Route to Dinuclear Mn-Complexes

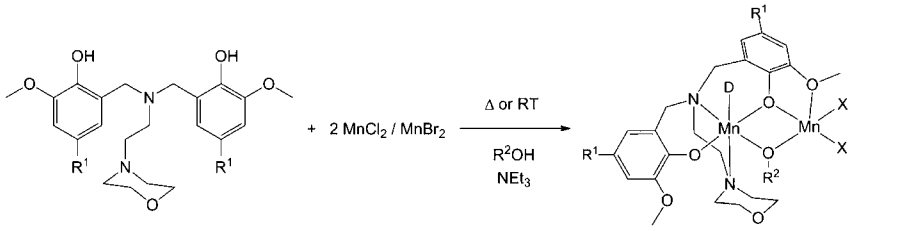

H_2L1 : $R^1 = CH_2CHCH_2$
H_2L2 : $R^1 = Me$

1 : $R^1 = CH_2CHCH_2$, $R^2 = Me$, D = MeOH, X = Cl
2 : $R^1 = Me$, $R^2 = Me$, D = MeOH, X = Cl
3 : $R^1 = CH_2CHCH_2$, $R^2 = Et$, D = EtOH, X = Cl
4 : $R^1 = Me$, $R^2 = Et$, D = Morph-O, X = Cl
5 : $R^1 = CH_2CHCH_2$, $R^2 = Me$, D = MeOH, X = Br
6 : $R^1 = Me$, $R^2 = Me$, D = MeOH, X = Br

temperature it was concentrated to ca. 5 mL by rotary evaporator and after which the formed dark green precipitate was separated by filtration. X-ray diffraction quality crystals were formed from slow evaporation of solution with the above-mentioned molar amounts at room temperature. Yield: 81 mg (50%). Elemental analysis: $C_{30}H_{43}Br_2Mn_2N_2O_7$ (813.36): calcd. C 44.30, H 5.33, N 3.44; found C 43.68, H 5.28, N 3.33.

Complex **6** was synthesized by dissolving 0.4 mmol (115 mg) of $MnBr_2{\cdot}4H_2O$ into 10 mL of methanol and 0.2 mmol (86 mg) of H_2L2 was added to the solution. Then, 0.4 mmol (56 μL) of triethylamine was added to neutralize the formed hydrobromic acid and the mixture was heated at 65 °C for 4 h. After the solution had cooled to room temperature it was concentrated to ca. 5 mL by rotary evaporator and after which the formed dark green precipitate was separated by filtration. X-ray diffraction quality crystals were formed from slow evaporation of solution with the above-mentioned molar amounts at room temperature. Yield: 81 mg (53%). Elemental analysis: $C_{26}H_{39}Br_2Mn_2N_2O_7$ (761.28): calcd. C 41.02, H 5.16, N 3.68; found C 41.14, H 5.13, N 3.57.

Complexes **7** and **8**: The single crystals of these complexes could be prepared by dissolving 0.02 mmol of **1** into methanol and adding 0.04 mmol of NH_4NO_3 (**7**) or NaOAc (**8**) to the solution and stirring the solutions for a few minutes. Crystals formed after slow evaporation of the solvent at room temperature. Despite several attempts we were unable to prepare these complexes in a larger scale.

Complex **9**: 0.09 mmol (68 mg) of complex **1** was dissolved into 6 mL of acetonitrile, and 0.3 mmol (17 μL) of ethylene glycol and 0.6 mmol (84 μL) of triethylamine were added. The mixture was left to crystallize at room temperature for two days and after which formed X-ray quality crystals were separated by filtration. Yield: 36 mg (60%). Elemental analysis: $C_{62}H_{82}Cl_2Mn_3N_6O_{12}$ (1339.07) (with 2 MeCN): calcd. C 55.61, H 6.17, N 6.28; found C 54.97, H 6.00, N 6.41.

X-ray Crystallography. The crystal data for compounds **1**–**10** are summarized in Table 1 along with other experimental details. The crystallographic data for **1**–**6** and **9** were collected at 123 K with an Enraf Nonius Kappa CCD area-detector diffractometer with the use of graphite-monochromated Mo-Kα radiation (λ = 0.71073 Å). Data collection was performed by using φ and ω scans, and the data were processed by using DENZO-SMN v0.93.0.[17] SADABS[18] absorption correction was applied for the compounds. For complexes **7**, **8**, and **10** the data collection was performed with Agilent SuperNova dual wavelength diffractometer equipped with an Atlas CCD area detector using Cu-Kα radiation using CrysAlisPro program package.[19] The empirical (**7** and **8**) absorption correction with SCALE3 ABSPACK scaling algorithm or analytical numeric one using multifaceted crystal (**10**) was performed as implemented in the CrysAlisPro program.

The structures were solved by direct methods by using the SHELXS-97[20] program or the SIR-97[21] program, and the full-matrix least-squares refinements on F^2 were performed using the SHELXL-97[20] program. Figures were drawn with Diamond 3.[22] For all compounds the heavy atoms were refined anisotropically. The CH hydrogen atoms were included at the calculated distances with fixed displacement parameters from their host atoms (1.2 or 1.5 times of the host atom). The OH hydrogens were located from the electron density map and refined isotropically.

RESULTS AND DISCUSSION

Synthesis. The ligands H_2L1 and H_2L2 were prepared in good to excellent yields by using a recently reported thermal oven method.[23] In general, the mixed-valence complexes **1**–**6** were synthesized according to Scheme 1, in which 2 equiv of $MnCl_2{\cdot}6H_2O$ (**1**–**4**) or $MnBr_2{\cdot}4H_2O$ (**5**–**6**) react with 1 equiv of the corresponding ligand in the presence of 2 equiv of triethylamine in a selected alcohol. As indicated previously by other authors,[24] in basic solutions under air, the coordination of the tetradentate tripodal ligands similar to H_2L1 and H_2L2 to Mn(II) species favors formation of Mn(III) species. The further reaction in a 1:1 molar ratio between the mononuclear Mn(III) intermediate and $Mn(II)X_2$ species present in the reaction medium gave rise to the formation of the $Mn^{II}Mn^{III}$ mixed-valence complexes.

In the syntheses of complexes **1** and **2**, best yields were obtained by heating the reacting solutions in methanol for 30–45 min, after which the solutions were allowed to cool to room temperature and the precipitate (for **1**) was filtered or the complexes (for **2**) were allowed to crystallize for a certain time to increase the yield and then were separated by filtration. A similar procedure as for **1** was also used for synthesis of **3.** For complex **4**, however, a better quality product was achieved with ultrasound assisted synthesis, when the starting materials (in ethanol) were placed in a ultrasound bath at room temperature for half an hour, took off from the bath and left to crystallize for two days after which the formed crystals were filtered. Complexes **5** and **6** were prepared by similar procedures as for **1** and **2** by using $MnBr_2{\cdot}4H_2O$ as the metal salt. The reactivity of **1**–**6** is discussed in detail later in the text.

The diffuse reflectance spectra of complexes **1**–**6** (Figure S8) show intense bands with a shoulder in the ultraviolet region at ~270 and ~320 nm, which are more likely due to intraligand and/or Mn(III)-ligand charge transfer bands. In the visible region these compounds exhibit a shoulder and a wide band at ~420 and ~700 nm, respectively. Since the high-spin Mn^{2+} ions have a d^5 configuration without spin-allowed bands in the visible region, these two bands come from the Mn^{3+} ion with tetragonally elongated octahedral geometry due to the presence of a strong Jahn–Teller effect. The band with a maximum at ~700 nm is assigned to the $^5A_{1g} \leftarrow {}^5B_{1g}$ transition, whereas the shoulder at ~420 nm can be tentatively assigned to the non-resolved $^5B_{2g} \leftarrow {}^5B_{1g}$ and $^5E_g \leftarrow {}^5B_{1g}$ transitions, which have their origin in the splitting of the $^5T_{2g}$ excited state of the O_h geometry. The positions of these bands are similar to those found for other

dx.doi.org/10.1021/ic302731z | Inorg. Chem. 2013, 52, 2228–2241

tetragonally distorted Mn^{3+} complexes.[25] The diffuse reflectance spectrum of **9** (Figure S8) exhibits one intense band at 250 nm and a band without clear maximum at 640 nm. The blue shift of the $^5A_{1g} \leftarrow {}^5B_{1g}$ transition with respect to its position in complexes **1**−**6** may be due to the higher Jahn−Teller distortion affecting complex **9**. It should be noted that no strong absorption assignable to an intervalence charge transfer was observed in the visible or near-IR region.

A direct evidence of the existence of Mn(II) and Mn(III) species is provided by XPS measurement. The deconvoluted XPS spectra of **1**−**6** are all almost identical, and, therefore, only that of compound **3** is given as an example in Figure 2. The

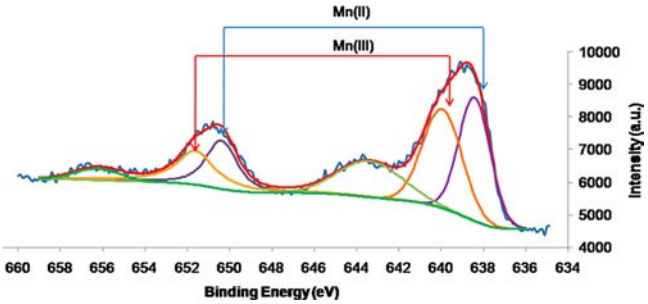

Figure 2. XPS spectrum for **3**.

spectrum shows peaks of $Mn2P_{3/2}$ and $Mn2P_{1/2}$ at 638.4 and 650.4 eV attributable to Mn(II), whereas the peaks at 639.9 and 651.6 eV indicate the presence of Mn(III). The contour area of the peaks clearly indicates the same content of Mn(II) and Mn(III). On the other hand, the XPS spectrum of compound **9** (Figure S9) shows the Mn(II) and Mn(III) peaks at bonding energies very close to those found for compounds **1**−**6**, but in this case the contour area of the peaks indicates a 2:1 Mn(III)/Mn(II) ratio.

X-ray Diffraction Analysis. The molecular structures of all studied complexes were determined by single crystal X-ray diffraction, and that of complex **1** is depicted in Figure 3 (for

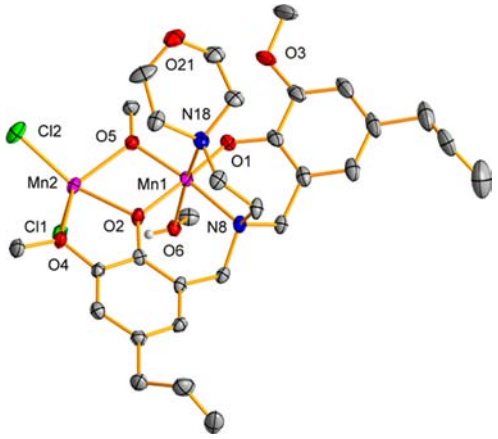

Figure 3. Molecular structure of complex **1**. Thermal ellipsoids have been drawn at the 30% probability level and C−H hydrogen atoms are omitted for clarity.

the molecular structures of **2**−**6**, see Figures S1−S3). The basic structure of all complexes **1**−**6** contains Mn(II) and Mn(III) ions, one aminobis(phenolato) ligand, one bridging alkoxo group, and two terminal halides. The Jahn−Teller distorted Mn(III) ion (D_{4h}) in all complexes is hexacoordinated with elongated octahedral coordination sphere which comprises one coordinated phenoxo oxygen, two tripodal nitrogens, one μ_2-bridging phenoxo group from the ligand, and one μ_2-bridging alkoxo oxygen. The sixth coordination site of Mn(III) ion is occupied either by a coordinated alcohol molecule (**1**−**3**, **5** and **6**) or by the morpholine oxygen (**4**) coming from a neighboring complex (see below). In the six-coordinated Mn(III) ions O1, N8, O2, and O5 donor form equatorial bonds to the metal ion (1.840−2.114 Å), and O6 and N18 form axial bonds (2.318−2.423 Å). The calculation of the degree of distortion of the Mn^{3+} coordination polyhedron with respect to ideal six-vertex polyhedra, by using the continuous shape measure theory and SHAPE software,[26] led to shape measures relative to the octahedron (OC-6) and trigonal prism (TPR-6) with values in the 1.6−2.1 and 14.2−15.4 ranges, respectively (see Table S3) Therefore, the Mn^{3+} coordination spheres are found in the OC-6 ↔ TPR-6 deformation pathway and are close to the octahedral geometry (∼90%) somewhat distorted to trigonal prismatic (see Table 3).

The pentacoordinated Mn(II) ions has in turn a distorted square based pyramidal coordination (Table 3), and it is surrounded by two terminal chlorides (**1**−**4**) or bromides (**5**−**6**), one μ_2-bridging phenoxo (O2), one μ_2-bridging alkoxo (O5), and one methoxy oxygen (O4) from the ligand. The other methoxy group (on the side of the hexacoordinated manganese) does not coordinate to the metal ion in any of the studied complexes.

Important geometrical parameters of complexes **1**−**6** are summarized in Tables 2 and S1. The bond distances around manganese atoms in all complexes are comparable to earlier studies concerning similar complexes.[15,24] The bonds from Mn(III) ion to phenoxo and alkoxo oxygens are about 0.2 Å shorter than those from Mn(II) ion to the same atoms, which furthermore confirms the different oxidation states between the two ions. The Mn1−O1 distance is slightly shorter than the Mn1−O2 one because the O2 is the bridging atom between the two manganese ions. In addition, the Mn1−N18 bond is considerably longer (usually more than 0.3 Å) compared to the other manganese nitrogen bonds (Mn1−N8) which is due to the Jahn−Teller effect of the Mn(III) ion.

The change of bridging alkoxo group from methoxo (**1**) to ethoxo (**3**) certainly has influence on the Mn−O5 bond lengths but also to other bonds around manganese ions which in turn causes variation on the Mn−Mn distance and the Mn−O−Mn angle. Generally the bond lengths between different complexes are similar whereas the bond angles have more deviation. Since complexes **5** and **6** are similar to **1** and **2** with terminal chlorides substituted with bromides, the structural parameters of the corresponding complexes are almost identical (excluding the Mn−Br bonds). However, there are small differences in Mn−O−Mn bond angles of **1** and **5** because of the different packing of the complexes (see below).

Solid State Packing. As the complexes provide several hydrogen bond acceptor atoms (chlorides coordinated to the Mn(II) ion, methoxy oxygens and aromatic rings in ligands) the packing of the complexes is mainly directed by these bonds and/or weak interactions. Interestingly, one of the most common donor atoms for these bonds is methylene or aromatic methoxy carbon atoms, whose charge distribution is polarized by neighboring nitrogen or oxygen atoms and aromatic rings, thus allowing these carbons to act as donor atoms in weak C−H···X hydrogen bonds.[27]

In complex **1** the OH proton of the coordinated methanol molecule has a strong intramolecular hydrogen bond to chloride (OH···Cl = 2.50 Å), whereas the same hydrogen in **2** has even stronger (2.39 Å) intermolecular hydrogen bond to the chloride ion of the neighboring molecule. Furthermore, complex **2** possesses an

dx.doi.org/10.1021/ic302731z | Inorg. Chem. 2013, 52, 2228−2241

Table 2. Selected Bond Lengths and Angles of 1−6

	1	2	3	4a[a]	4b[a]	5	6
Mn1−O1	1.846(2)	1.847(2)	1.857(2)	1.861(5)	1.858(5)	1.840(5)	1.853(4)
Mn1−O2	1.915(2)	1.934(2)	1.903(2)	1.924(5)	1.905(5)	1.912(5)	1.933(4)
Mn1−O5	1.902(2)	1.900(2)	1.912(2)	1.889(6)	1.927(6)	1.902(5)	1.904(4)
Mn1−N8	2.092(3)	2.095(2)	2.090(2)	2.110(7)	2.082(6)	2.114(6)	2.095(5)
Mn1−O6	2.319(2)	2.320(2)	2.323(2)			2.318(5)	2.329(4)
Mn1−N18	2.413(3)	2.423(2)	2.402(2)	2.357(6)	2.413(6)	2.408(6)	2.411(4)
Mn1−O21′				2.414(5)	2.484(5)		
Mn2−O2	2.109(2)	2.112(2)	2.127(2)	2.160(5)	2.146(6)	2.123(5)	2.100(4)
Mn2−O4	2.433(2)	2.464(2)	2.416(2)	2.422(6)	2.379(6)	2.409(5)	2.476(4)
Mn2−O5	2.127(2)	2.118(2)	2.147(2)	2.152(6)	2.155(6)	2.106(5)	2.115(4)
Mn2−Cl1	2.309(1)	2.338(1)	2.385(1)	2.340(2)	2.349(2)	2.497(2)[b]	2.484(1)[b]
Mn2−Cl2	2.358(1)	2.360(1)	2.326(1)	2.332(2)	2.345(2)	2.480(2)[c]	2.501(1)[c]
Mn1−Mn2	3.1726(6)	3.1777(5)	3.2061(4)	3.2188(16)	3.243(2)	3.1848(15)	3.1733(12)
Mn1−O2−Mn2 (θ)	104.0(1)	103.4(1)	105.3(1)	103.9(2)	106.2(2)	104.1(2)	103.7(2)
Mn1−O5−Mn2 (θ)	103.8(1)	104.4(1)	104.2(1)	105.4(2)	105.1(2)	105.1(2)	104.2(2)
Mn1−O2−O5−Mn2	171.8(1)	177.1(1)	171.8(1)	176.5(3)	177.9(3)	175.1(2)	176.5(2)
O2−Mn1−Mn2−O5	169.5(1)	176.2(1)	169.4(1)	175.5(4)	177.2(4)	173.7(3)	175.6(3)

[a]The geometrical parameters of two different dinuclear complexes in the asymmetric unit of **4** are presented as 4a and 4b. [b]Mn1−Br1. [c]Mn1−Br2.

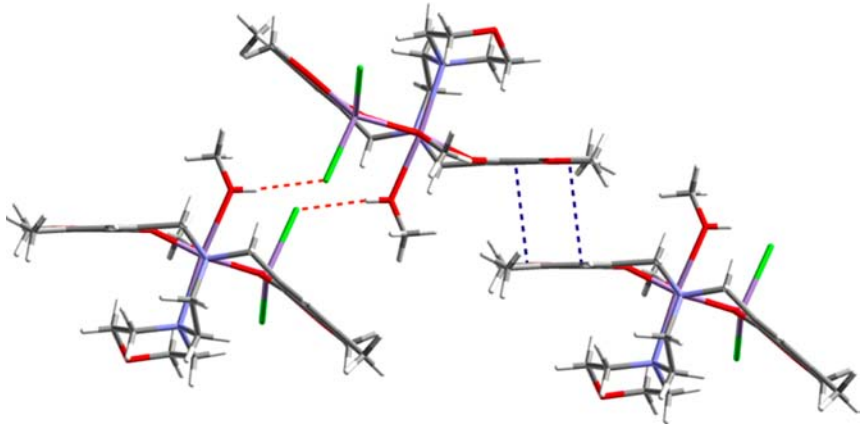

Figure 4. Solid state packing of complex **2** showing the intermolecular hydrogen bonding (red) and $\pi-\pi$ interaction (blue).

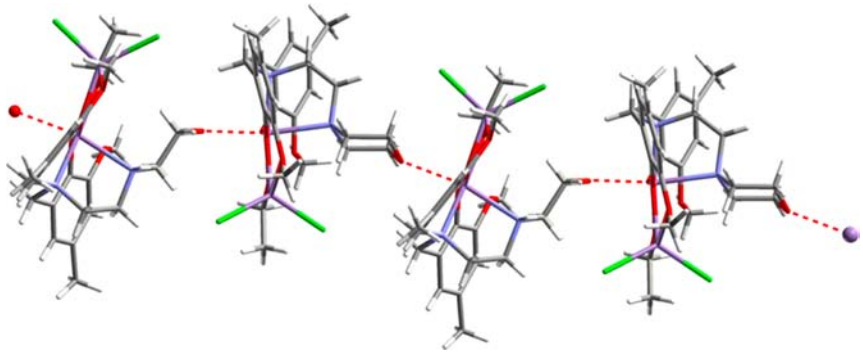

Figure 5. The packing diagram of **4** showing the 1D polymeric structure.

example of parallel offset aromatic−aromatic ($\pi-\pi$) interaction with two phenyl rings lying partly on top of each other with a separation of 3.38 Å. The preceding interaction and/or strong intermolecular OH···Cl hydrogen bonds mainly determines the spatial arrangement of **1** and **2** in the lattice (Figure 4). Both complexes have also several rather weak intermolecular interactions between chlorides and methylene, aromatic and/or methoxy methyl hydrogens, which further facilitate the crystallization by stabilizing the entire structure.

The packing of complex **3** is fairly similar to that of **1** with strong intramolecular hydrogen bonds from coordinated ethanol to chloride and slightly weaker intermolecular interactions to chloride and morpholine oxygen from methylene and aromatic hydrogens.

The solid state ordering of **4** differs from the preceding complexes notably since the coordinated alcohol molecule observed in previous complexes has been replaced by a morpholine oxygen from the adjacent complex filling the coordination sphere of Mn(III) ion (Figure 5). This induces significant changes in the

dx.doi.org/10.1021/ic302731z | Inorg. Chem. 2013, 52, 2228−2241

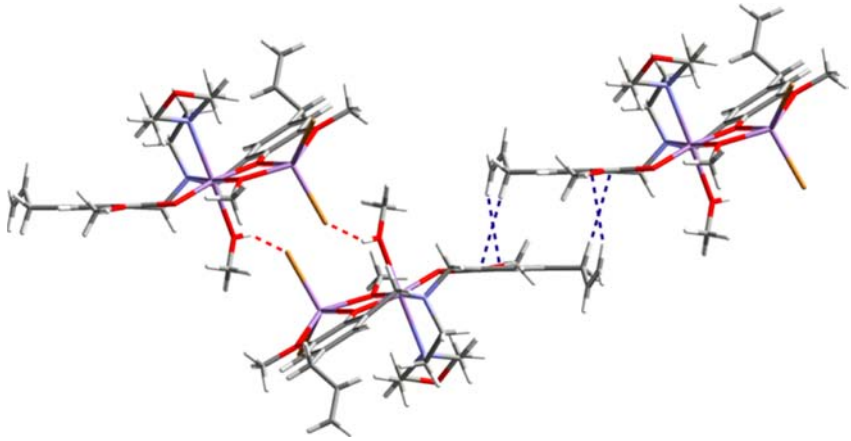

Figure 6. The solid state ordering of complex **5** showing the intermolecular OH···Br- (red) and CH···π-hydrogen bonds (blue).

Scheme 2. Schematic Pathway for the Formation of Complexes 7−9

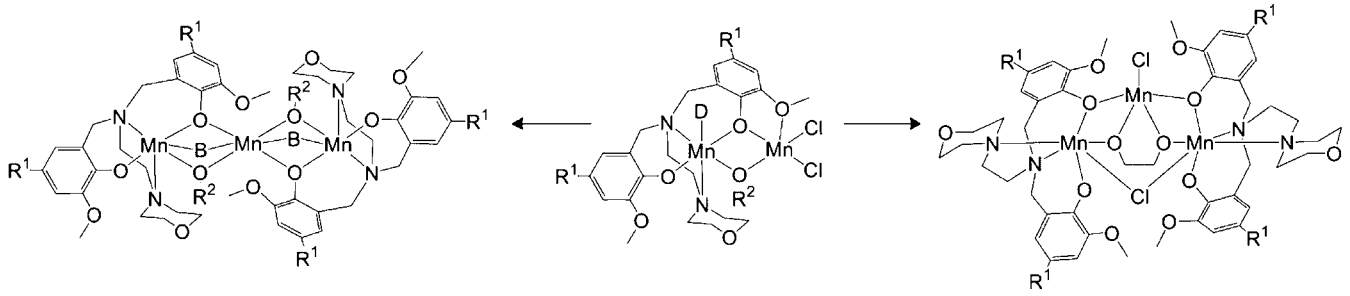

orientation of the whole morpholine ring compared to complexes **1**−**3** in which the morpholine ring has settled nearly parallel compared to the Mn−O−Mn−O plane, whereas in **4**, the ring is virtually orthogonal to this plane. The coordination of the morpholine oxygen produces a 1D coordination polymer with fairly few interactions to two other directions. Besides the aforementioned interaction, one notable intermolecular contact is between a hydrogen from the methoxy group and the methoxy oxygen from an adjacent complex (with C···O separation of 3.38 Å).

Rather surprisingly, the packing of complex **5** is reminiscent of complex **2** more than **1** (which has the same ligand, H_2L1), with strong intermolecular H···Br hydrogen bonds instead of intramolecular ones. The packing of complexes **6** and **2** is almost identical (although the aromatic−aromatic interaction is not as clear as in **2**). The stacking of aromatic rings in both complexes **5** and **6** is probably best described as CH/π hydrogen bond than actual π−π interaction (Figure 6).

Reactivity of the Complexes. We were interested in the reactivity of the synthesized complexes in order to be able to prepare more complicated molecular structures with larger spin ground state and easy-axis (Ising type) magnetic anisotropy, the most sought-after properties of SMMs. From the solid state structures of **1**−**6**, chemical intuition would suggest that the coordinated halides would be the most reactive groups in these complexes; hence the lability of the complexes toward anion exchange reactions using sodium and ammonium salts of some common anions was investigated.

The reactivity was initially tested with ammonium nitrate by stirring complex **1** and 2 equiv of NH_4NO_3 in methanol for 4 h. Unfortunately, precipitation or crystal formation from the solution was not observed even at −20 °C. However, small amounts of single crystals suitable for X-ray diffraction were formed after very slow evaporation of methanol solution. The solid state structure revealed that the nitrate group has indeed replaced the chloride ions. However, since the coordination capability of the nitrate as a monodentate ligand is weaker than the chloride, instead of the formation of the assumed $Mn_2L^1\mu_2$-$OMe(NO_3)_2$ complex, the reaction unexpectedly proceeded further to produce the mixed-valence trinuclear Mn(III)/Mn(II)/Mn(III) complex **7** (Scheme 2). The distorted octahedral coordination sphere of both Mn(III) ions in **7** is similar to **1** and **2** by means of amino(phenolate) ligand coordinated in a tetradentate manner and Mn(III)/Mn(II) μ_2-bridging methoxo group. The μ_2-bridging nitrate anions have replaced the chlorides, aromatic methoxy substituents, and/or coordinated alcohol/morpholine oxygens around the manganese ions, thus producing a distorted octahedral coordination sphere for all metal ions in the complex (for geometrical parameters, see Table S2).

The above-described procedure with complex **1** and sodium acetate produced complex **8** (Figure 7) with acetate anions as bridging ligands. The coordination sphere around metal ions is similar to **7**, although the geometrical parameters around them are somewhat different (Table S2). In spite of our numerous efforts with several solvents and starting materials, we have not been able to produce pure enough bulk material from these reactions, and hence the magnetic properties of complexes were studied only by computational methods (see below). However, the obtained crystal structures demonstrate that coordinated halides are reactive and can be replaced by different anions.

dx.doi.org/10.1021/ic302731z | Inorg. Chem. 2013, 52, 2228−2241

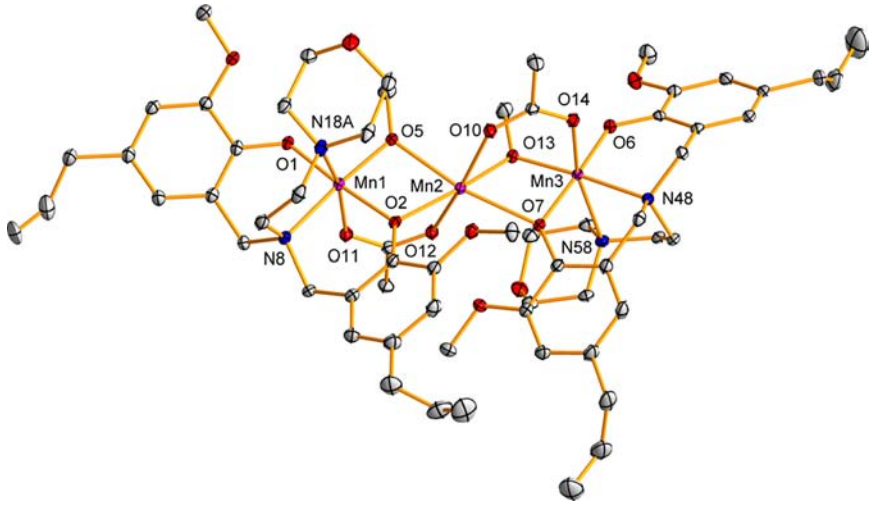

Figure 7. Molecular structure of **8**. Thermal ellipsoids have been drawn at 30% probability level and C−H hydrogen atoms are omitted for clarity.

Another interesting reaction for the prepared dinuclear complexes would be the substitution reaction of the halides by an alcoholate with the aim to get a new complex with an additional alkoxo ligand coordinated to the metal ion. Thus, we explored the possible reaction between complexes **1**−**4** and 10-fold excess of ethylene glycol in the presence of triethylamine expecting that the ethylene glycolate dianion coordinates to the Mn(II) ion in a bidentate manner by replacing the chloride ions. The reaction in acetonitrile rapidly produced a green precipitate, but we were not able to recrystallize it to achieve any X-ray diffraction quality crystals. However, the same reaction with complex **3** proceeded more slowly, thus producing green, good quality crystals of **9** from which we were able to determine the structure of the product (Figure 8).

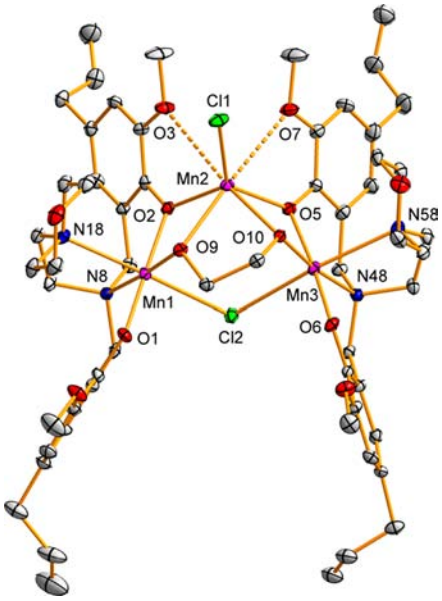

Figure 8. Molecular structure of **9**. Thermal ellipsoids have been drawn at 30% probability level and hydrogen atoms and non-coordinating solvents are removed for clarity.

Nevertheless, crystals did not consist of the expected ethylene glycolate adduct, but quite surprisingly we found again a trinuclear Mn(III)/Mn(II)/Mn(III) complex (**9**), with a Mn(1)−Mn(2)- and Mn(2)−Mn(3)-μ_2-bridging ethylene glycolate, Mn(1)−Mn(3)-μ_2-bridging chloride anion and one additional terminal chloride coordinated to the central Mn(2)-ion (Scheme 2, Figure 8). Both Mn(III) cations have Jahn−Teller distorted octahedral coordination spheres with tetradentally coordinated ligand $L3^{2-}$ replenished with bridging chloride and alkoxo oxygen, while the surroundings of the Mn(II) ion vaguely resemble those in **1**−**6** with two pairs of bridging alkoxo and phenoxo oxygens and terminal chloride anion. The bridging chloride anion between the Mn(III) cations causes the whole structure to be folded (the Mn(1)−Cl(2)−Mn(3) angle is 111.8°) compared to the rather linear arrangement in **7** and **8**. Selected geometrical parameters of **9** can be found in Table S2.

In the absence of triethylamine the reaction produces complex **10** where the original alkoxo bridge has been replaced by just singly deprotonated ethylene glycol (Figure S5); hence triethylamine is presumably needed for the double deprotonation of ethylene glycol enabling the trinuclear product. Later, we were able to grow crystals from the reaction of **1** and ethylene glycol, thus confirming that also the methoxo bridged complexes undergo the preceding reaction and the bulk material was prepared using **1** as the starting material.

On considering the remarkable reactivity of these dinuclear Mn(II)/Mn(III) complexes, we should be able to push these complexes to react with another alcohol (or acids) to produce differently bridged systems. It seems that we can transform **1** into **3** by dissolving it in ethanol and exchange the methoxo bridge to monodentate μ_2-bridging ethylene glycol (**10**), which gives us additional support on the reactivity of the alkoxo bridge. The previously mentioned reactions pointed out how rich the chemistry of complexes **1**−**6** can be, and we are currently working to selectively change the bridging group and exploring new reactions to produce complexes with higher nuclearities.

Magnetic Properties. Variable-temperature magnetic susceptibility studies were carried out on powdered samples of the crystalline complexes **1**−**6** and **9** in the temperature range 2−300 K and under an applied field of 1000 Oe. The magnetic properties of compounds **1**−**6** and **9** in the form of $\chi_M T$ vs T plots (χ_M being the magnetic susceptibility per $Mn^{II}Mn^{III}$ unit for compounds **1**−**6**, and per $Mn^{III}Mn^{II}Mn^{III}$ unit for compound **9**) are shown in Figure 9.

dx.doi.org/10.1021/ic302731z | Inorg. Chem. 2013, 52, 2228−2241

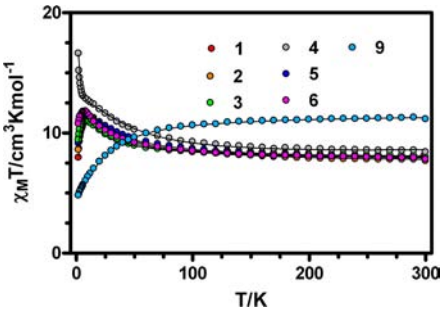

Figure 9. Temperature dependence of the $\chi_M T$ product for complexes **1**–**6** and **9**.

For compounds **1**–**6**, the value of $\chi_M T$ at room temperature is slightly higher than the theoretical value (7.375 cm^3 mol^{-1} K) expected for a dinuclear system with magnetically isolated Mn^{2+} (S = 5/2, g = 2) and Mn^{3+} ions (S = 2, g = 2). When the temperature is lowered, the $\chi_M T$ steadily increases reaching a maximum (a shoulder in the case of **4**) of ~12 cm^3 mol^{-1} K at ~10 K. Below this temperature, the $\chi_M T$ decreases rapidly to 2 K (in the case of **4** the $\chi_M T$ sharply increases to reach a value of 16.6 cm^3 K mol^{-1} at 2 K). This behavior is due to a significant intradinuclear ferromagnetic coupling between Mn^{2+} and Mn^{3+} ions leading to a S = 9/2 ground state. The decrease in $\chi_M T$ at low temperatures for compounds **1**–**3** and **6** suggests the existence of zero field splitting (ZFS) effects due to the presence of an anisotropic Mn^{3+} ion (the ZFS for the isotropic Mn^{2+} ion is assumed to be comparatively negligible) and/or intermolecular antiferromagnetic interactions. In the case of **4**, the sharp increase in $\chi_M T$ at low temperature is due to intermolecular ferromagnetic interactions. At room temperature, the $\chi_M T$ value for **9** (11.23 cm^3 K mol^{-1}) is very close to the expected value for a magnetically uncoupled system containing two Mn^{3+} ions and one Mn^{2+} ion with g = 2.11 (11.42 cm^3 mol^{-1} K). On lowering temperature, the $\chi_M T$ first decreases slowly until ~100 K and then sharply to reach a value of 4.75 cm^3 mol^{-1} K at 2 K. The shape of this curve is typical of a dominant antiferromagnetic coupling in the trinuclear complex **9**.

In keeping with the dinuclear structure of the $Mn^{II}Mn^{III}$ mixed-valence complexes the magnetic susceptibilities of complexes **1**–**6** were analyzed by means of the following the spin exchange Hamiltonian:

$$H = -J\mathbf{S_1}\mathbf{S_2} - D_{Mn}(\mathbf{S_z^2} - 2) + zJ' < S_z > \mathbf{S_z}$$

with (S_1 = 2 and S_2 = 5/2). The second term describes the local anisotropy of the Mn^{3+} ion and the third term describes the intermolecular interactions in the molecular field approximation.[28] Because D and zJ' are strongly correlated, as they produce the same effect on the experimental curves (a decrease in the $\chi_M T$ product at low temperature), their independent contributions cannot be reliably evaluated from the magnetic susceptibility data. In view of this, we decided to fit the experimental magnetic susceptibility with the above Hamiltonian but fixing either D or zJ' to zero. However, in the first case, the corresponding fits lead to unacceptable high values of D. Therefore, we will keep the magnetic parameters extracted with D_{Mn} fixed to zero, which are gathered in Table 3, for further discussions. It should be noted that the zJ' parameters obtained from the fitting procedure are overestimated as they include the effects of both the weak intermolecular interactions and the local anisotropy of the Mn^{3+} ion. In the case of the chain complex **4**, the binuclear subunits are far away from each other, so that the magnetic interaction between the two dinuclear units can also be analyzed with the molecular field approximation. To avoid overparametrization, the two different dinuclear units present in **4** were considered to have the same magnetic coupling.

In order to support the experimental J values found for compounds **1**–**6** and to determine some magnetic interactions that could not be extracted from the fitting of the magnetic data, density functional theory (DFT) calculations using the broken-symmetry approach (see Supporting Information) were

Table 3. Magnetostructural Data for the Mixed-Valence $Mn^{II}Mn^{III}$ Complexes 1–9

complex	1	2	3	4	5	6	7	8	9
***J* calcd/cm^{-1}**									
J1–2	+10.4	+13.4	+10.0	+10.7/+12.4[a]	+12.7	+12.6	+5.9[e]	+7.9[f]	+3.1[g]
J2–3				−0.02[b]			+2.4	+7.9	+0.52
J1–3				+0.02/−0.01[c]			−0.37	−0.44	−8.6
J1–4				<0.01[d]					
***J* exp/cm^{-1}**									
J1–2 (J1′-2′)	+3.44(6)	+4.2(1)	+2.15(6)	+7.9(7)	+3.7(1)	+2.9(1)			0.04(7)
J2–2′									−5.3(1)
g	2.045(2)	2.012(4)	2.032(3)	1.993(1)	2.049(5)	2.042(3)			2.11(1)
zJ'	−0.10(1)	−0.06(1)	−0.07(1)	−0.04(1)	−0.08(1)	−0.04(1)			
θ/(°)[i]	103.88	103.90	104.73	105.15	104.61	103.93	100.68	102.65	101.63
Mn^{2+}-Mn^{3+}/Å[i]	3.179	3.178	3.206	3.231	3.185	3.173	3.189	3.181	3.191
distortion[h]	9.3	7.2	14.4	2.4	2.3	6.8			17.3
from C_{4v} (δ, %)				11.7					
distortion	9.3	10.3	9.6	11.5[i]	10.3	10.5	9.4[i]	11.6	13.1
from O_h (%)[j]									

[a]The pair of values refers to both dinuclear subunits forming the tetranuclear complex (see Figure S10). The first value is for the dinuclear moiety with Mn^{II}–Mn^{III} distance at 3.219 Å, and the second, to the other subunit, with Mn^{II}–Mn^{III} distance of 3.243 Å. [b]This value is for the coupling between the two dinuclear subunits connected throughout the Mn^{III} metallic centers. [c]This value refers to the two possible 1,3 Mn^{II}/Mn^{III} magnetic coupling. [d]This value is for the 1,4 Mn^{II}/Mn^{II} magnetic coupling. [e]This value is for the pair Mn^{III}/Mn^{II} at 3.182 Å (below appears the value for the Mn^{III}/Mn^{II} pair at 3.196 Å). [f]This complex is centrosymmetric. [g]This value is for the pair Mn^{III}/Mn^{II} at 3.216 Å (below appears the value for the Mn^{III}/Mn^{II} pair at 3.166 Å). [h]Distortion from SPY-5 toward TPBY-5 calculated using the Addison's method: $\delta = (\beta-\alpha)/60$, α and β are the largest *trans* bond angles; see ref 29. [i]Average values. [j]Distortion from OC-6 toward TPR-6 calculated using the SHAPE program.[26]

dx.doi.org/10.1021/ic302731z | *Inorg. Chem.* 2013, 52, 2228–2241

carried out on the X-ray structures as found in the solid state. As it can be observed in Table 3, the calculated values are in good agreement in sign and magnitude with those obtained from the experimental results.

The field dependences of the molar magnetization at 2 K for compounds **1**−**6** (the *M* vs *H* plot for compound **3** is given as an example in Figure 10) are below the Brillouin function for $S = 9/2$,

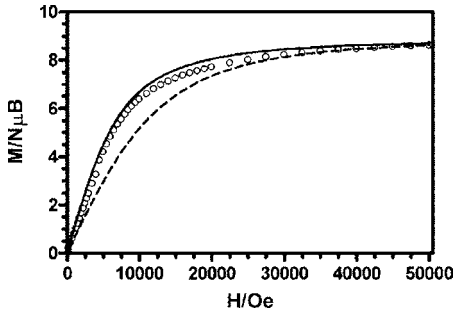

Figure 10. *M* vs *H* plot for **3**. The solid and dashed lines represent the Brillouin functions for a $S = 9/2$ ground state and for the sum of a $S = 2$ and a $S = 5/2$ spin states with $g = 2.03$, respectively.

which is more likely due to the combined effects of interdimer antiferromagnetic interactions and/or zero-field splitting of the $S = 9/2$ ground state. However, the experimental values are well above the sum of the magnetization contributions expected for the isolated ions, thus supporting the intramolecular ferromagnetic interaction in these compounds.

Variable-temperature magnetization data were collected between 2 and 10 K at applied fields ranging from 0.5 to 7 T. The *M* vs *H*/*T* plots for **1**−**6** (the plot for compound **3** is given as an example in Figure 11) are not superimposed on a

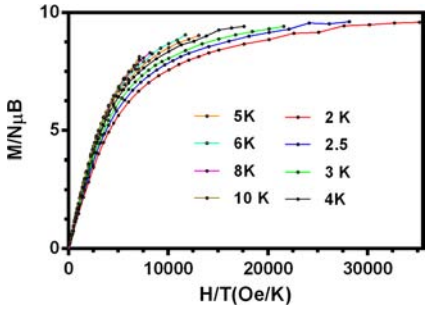

Figure 11. *M vs H*/*T* plots for **3**. Solid lines are guides for the eye.

single master curve, clearly indicating the presence of a significant magnetic anisotropy in these complexes. However, all attempts to obtain the *D* and *E* anisotropic parameters of the $S = 9/2$ ground state by fitting the reduced magnetization data were unsuccessful.

The sign and magnitude of the ferromagnetic exchange interactions in $Mn^{II}Mn^{III}$ mixed valence pairs can be understood using the known Goodenough−Kanamori rules,[30] which state that the magnetic exchange interactions between pairs of overlapping magnetic orbitals are antiferromagnetic, those between pairs of orthogonal magnetic orbitals are ferromagnetic, and those due to the overlapping of the magnetic orbital of an ion with an empty orbital of another ion are ferromagnetic through the spin polarization mechanism. For the sake of simplicity, let us assume that Mn^{2+} and Mn^{3+} ions have square pyramidal (C_{4v}) and ideal elongated octahedral (D_{4h}) geometries, respectively. The five *d*-type orbitals span the irreducible representations of the corresponding symmetry group and split as shown in Figure 12. For the Mn^{2+} ion all the

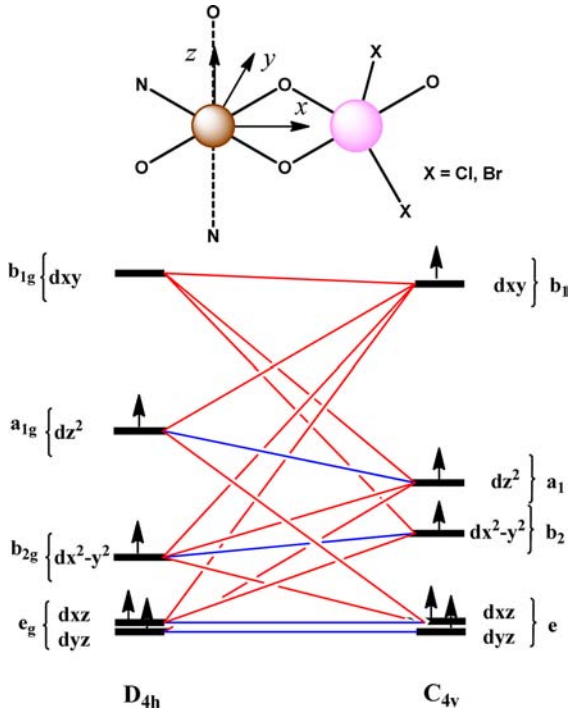

Figure 12. Magnetic exchange pathways in $Mn^{II}Mn^{III}$ mixed-valence dinuclear complexes. Red and blue lines represent the ferromagnetic and antiferromagnetic interactions, respectively.

d orbitals are half-filled orbitals, whereas in the Mn^{3+} ion the $dxy(b_1)$ is an empty orbital and the rest are half-filled d orbitals. In the almost planar $Mn^{II}(O)_2Mn^{III}$ bridging fragment, the interaction between the magnetic orbitals of the Mn^{2+} and Mn^{3+} ions gives rise to a number of ferromagnetic (F) and antiferromagnetic (AF) competing contributions, the most significant occurring in the *xy* plane. Thus, the interaction between the empty *dxy* orbital of the Mn^{3+} ion and the half-filled, close in energy magnetic orbitals of the Mn^{2+} ion, the so-called crossed interactions (Jb_1b_2, Jb_1a_1 and Jb_1b_1 being the leading terms),[28] as well as the interaction between orthogonal orbitals (the leading terms being Jb_2b_1, Ja_1b_1, Je_gb_1, and Je_gb_2) is ferromagnetic. For θ bridging angles larger than 100°, the interaction between magnetic orbitals of the same symmetry is AF, such as Jb_2b_2, Ja_1a_1, Je_ge_g. This latter contribution concerns orbitals where the *xy* is a nodal plane, which are weakly delocalized toward the bridging oxygen atoms through π-type metal-bridging ligand overlap and therefore is expected to be very weak AF. The Ja_1a_1 involves orbitals that are weakly delocalized in the *xy* plane, and so a weak AF interaction is also expected. Finally, the Jb_2b_2 contribution deals with the dx^2-y^2 orbitals pointing toward each other along the *x*-axis and are weakly delocalized toward the bridges in a π-manner. Therefore, for $\theta > 100°$ a medium AF contribution is expected (this includes the direct overlap which is favored when θ is small). Although usually AF contributions are stronger than the F ones, in complexes **1**−**6** the relatively higher number of F contributions and the weakness of the AF contributions (all these complexes have $\theta > 100°$) could lead to a situation where

dx.doi.org/10.1021/ic302731z | Inorg. Chem. 2013, 52, 2228−2241

Table 4. Magnetostructural Data for Dinuclear and Trinuclear Mixed-Valence $Mn^{II}Mn^{III}$ Complexes[a]

compound	J_{exp}/cm^{-1}	$\theta/°$	$\beta/°$	geometry Mn^{II}/Mn^{III}	CCDC code	ref
Dinuclear						
Double triazolate bridges						
$[Mn^{II}Mn^{III}(L)_2(CH_3OH)_3(OCN)]\cdot(H_2O)_2$	+1.3	132.7[b]	16.1	OC-6/OC-6	OHIXEJ	31
$[Mn^{II}Mn^{III}(L)_2(H_2O)_2(phba)]\cdot(DMF)_2\cdot(CH_3OH)_{0.5}$	+2.3	131.6	36.3	OC-6/OC-6	OHIYAG	30
$[Mn^{II}Mn^{III}(L)_2(DMF)_{1.5}(H_2O)_{1.5}Cl]\cdot(H_2O)_{2.5}$	+1.7	132.2	27.6	OC-6/OC-6	OHIXUZ	30
$\{[Mn^{II}Mn^{III}(L)_2(CH_3OH)(H_2O)_2]_2(\mu\text{-fua})\}\{[Mn^{II}Mn^{III}(L)_2(CH_3OH)(H_2O)_2](\mu\text{-fua})\}\cdot 4CH_3OH\cdot 8H_2O$	+1.6	132.1/132.1	26.02/31.04	OC-6/OC-6	OHIXOT	30
$\{[Mn^{II}Mn^{III}(L)_2(DMSO)_2(H_2O)]_2(\mu\text{-suc})\}\cdot 10H_2O$	+1.2	133.5	27.8	OC-6/OC-6	OHIYEK	30
$\{[Mn^{II}Mn^{III}(L)_2(CH_3OH)_3]_2(\mu\text{-phth})\}\cdot CH_3OH\cdot 5H_2O$	+2.2	131.9	1.4	OC-6/OC-6	OHIXIN	30
$\{[Mn^{II}Mn^{III}(L)_2(H_2O)_2][Mn^{II}Mn^{III}(L)_2(CH_3OH)(H_2O)(DMF)]\}\cdot 5H_2O\cdot DMF\cdot CH_3OH$	+1.5	128.9/132.3[b]	55.84/27.30	OC-6/OC-6	OHIYIO	30
Phenoxo-alkoxo bridges						
$[Mn^{III}(L^1)(CH_3OH)(OCH_3)Mn^{II}Cl_2]\cdot CH_3OH$	+6.0	106.2/103.3	9.8	SPY-5/OC-6	CAFHOG	24a
Double diphenoxo bridges						
$[Mn^{II}Mn^{III}(biphen)_2(biphenH)(bpy)_2]$	+1.8	97.0/102.4	10.8	SPY-5/OC-6	GAVWOP	32
$[Mn^{II}Mn^{III}(L^2)(H_2O)_3](ClO_4)_2\cdot 1/2EtOH\cdot 1/4H_2O$	+2.9	99.1	9.8	OC-6/OC-6	LOBMOE	33
Double dialkoxo bridges						
$(TEA)[Mn^{II}Mn^{III}(2\text{-}OH(5\text{-}Clsal)pn)_2]$	+0.5	103.9	5.1	OC-6/OC-6	ROCRAC	34
Triple alkoxo/hydroxo/phenoxo dicarboxylate bridges						
$[Mn^{II}Mn^{III}(\mu\text{-}OH)\text{-}(\mu\text{-piv})_2(Me_3tacn)_2](ClO_4)_2$	−8.5	119.3		OC-6/OC-6	TIPFED	35
$[Mn^{II}Mn^{III}(bpmp)(\mu\text{-}OAc)_2](ClO_4)_2\cdot H_2O$	−6.0	114.4		OC-6/OC-6	FOSCAR	36
$[Mn^{II}Mn^{III}(bcmp)(\mu\text{-}OAc)_2](ClO_4)_2\cdot Cl_2CH_2$	−7.7	112.3		OC-6/OC-6	GACCOC	37
Triple diphenoxochloride bridges						
$[Mn^{II}Mn^{III}(L^3)(\mu\text{-}Cl)ClBr]$	−1.7	93.6/102.5	34.2	OC-6/OC-6	FOSCEV	35
Trinuclear						
Bisdialkoxo and bisalkoxophenoxo bridges						
$[Mn^{III}Mn_2{}^{II}(Hcht)_2(bpy)_4](ClO_4)_3\cdot Et_2O\cdot 2MeCN$	+3.2	102.0	0.0	OC-6/OC-6	WANHUP	38
$[Mn^{III}Mn_2{}^{II}(L^4)(\mu\text{-}OMe)_2](ClO_4)_3$	+3.6	96.8/108.0	6.9	OC-6/OC-6	QAXZUK	39
		96.6/107.7	9.1			
Triple Phenoxodicarboxylate						
$[Mn^{III}{}_2Mn^{II}(L^5)_2(ba)_4]$	−6.7	113.2/114.8		OC-6/OC-6	CAFNAY	24a
Triple Phenoxo-hydroxo-carboxylate						
$[Mn^{III}{}_2Mn^{II}(L^5)_2(dcba)_2(OMe)_2]$	−2.5	102.1/97.8	22.5	OC-6/OC-6	PUYMEB	40
Triple Phenoxo-alkoxo-carboxylate						
$[Mn^{III}{}_2Mn^{II}(L^6)_2(CH_3CH_2COO)_2(OMe)_2]\cdot H_2O$	−0.13	99.9/100.9	26.5/24.9	OC-6/OC-6	FORVEO	41
$[Mn^{III}{}_2Mn^{II}(L^7)_2(mcba)_2(OMe)_2]$	+3.8	102.9/99.2	24.5	OC-6/OC-6	NUJPEN	42

[a] H_2L = 3-(2-phenol)-5-(pyridin-2-yl)-1,2,4-triazole. Phba = *p*-Hydroxybenzoic. Fua = fumaric acid. Suc = succinic acid. Phth = terephthalic acid. H_2biphen = 2,2′-biphenol. Piv = pivalic acid. Me_3tacn = 1,4,7-trimethyltriazacyclonane. Bpmp = it was prepared from the condensation of bis[(2-pyridylmethyl)methyl]amine with 2,6-bis(chloromethyl)-*p*-cresol. H_2L^1 = *N*-(3,5-di-*t*-buthyl-2-hydroxybenzyl)-*N*-(2-hydroxy-3-methoxybenzyl)-*N*′,*N*′-dimethylethylenediamine. H_2L^2 = it was prepared form the condensation of 2,6-diformyl-4-methylphenol with diethylenetriamine and $ClCH_2COOEt$. 2-OH(5-Clsal)pn = 1,3-bis(salicylideneamino)-2-propanol. H_2L^3 = it was prepared form the condensation of 2,6-diformyl-4-*t*-butylphenol with 1,3-diaminepropane. Bcmp = prepared by the reaction of *N*,*N*′-bis(*p*-tolylsulfonyl)-1,4,7-tacn with 2,6-bis(chloromethyl)-*p*-cresol followed by deprotection. Hcht = *cis*,*cis*-1,3,5-cyclohexanetriol. H_2L^4 = it was prepared from the metal-templated Schiff-base condensation of 2,6-diformyl-4-methylphenol with 1,11-diamino-3,9-dimethyl-3,9-diazo-6-oxaundecane. H_2L^5 = *N*,*N*-bis(2-hydroxybenzyl)-*N*′,*N*′-dimethylethylenediamine and dcba = 2,6-dichlorobenzoic acid. H_2L^6 = *N*,*N*′-dimethyl-*N*,*N*′-bis(2-hydroxy-3,5-dimethylbenzyl)-ethylenediamine. H_2L^7 = *N*-(3,5-di-*t*-buthyl-2-hydroxybenzyl)-*N*-(2-hydroxybenzyl)-*N*′,*N*′-dimethylethylenediamine. Hmcba = *m*-chlorobenzoic. [b] Mean value of the Mn^{II}−N−N and Mn^{III}−N−N angles.

the F contributions were dominant. In fact, all the dinuclear and trinuclear $Mn^{II}Mn^{III}$ complexes containing a planar bridging network (diphenoxo, phenoxo/alkoxo, and dialkoxo bridges) exhibit ferromagnetic coupling (Table 4).

In those cases where the magnetic coupling is AF, there are additional bridges (usually *syn-syn* carboxylate groups) that slightly fold the structure affecting the magnitude of the AF and F competing interactions in such a way that the AF contributions become dominant. This AF behavior can be alternatively explained by considering the counter-complementarity exerted by the coordination of an additional *syn-syn* carboxylate group to the square planar $Mn^{II}(O)_2Mn^{III}$ bridging fragment, which induces a decrease in the ferromagnetic *J* value. The relatively low calculated *J* values for the trinuclear Mn^{III}−Mn^{II}−Mn^{III} complexes **7** and **8**, which contain triple alkoxo/phenoxo/acetate bridging groups, compared to those complexes **1**−**6**, support this hypothesis.

It should be pointed out that the magnetic coupling might also contain a contribution due to the spin-dependent delocalization (also called double exchange), which is always positive.[43] Whereas the superexchange takes place by electron transfer via an excited state, which is mixed into the ground state by second-order perturbation, the spin-dependent delocalization occurs via ground state configurations. In complexes **1**−**6**, the spin-dependent delocalization term, if it exists, is very small as the valences of the Mn^{2+} and Mn^{3+} are essentially trapped (class I compounds according to Robin and Day classification).

dx.doi.org/10.1021/ic302731z | Inorg. Chem. 2013, 52, 2228−2241

After analyzing the structural parameters for a series of dinuclear and trinuclear $Mn^{II}Mn^{III}$ mixed valence complexes, one can draw the following conclusion: Although the J values are not very sensible to the θ value, it seems that they increase when θ increases and the distortion of the Mn^{2+} polyhedron from ideal square pyramidal geometry decreases. Thus compound **3** with a comparatively large θ value and the larger distortion (δ = 0.14; δ is zero for SPY-5 and 1 for TBPY-5) exhibits the lower J value. However, compound **4** with the bigger θ values and less distortion in one of their different dinuclear units exhibits the stronger magnetic coupling. The calculated J values for **1**−**6** seem to follow the same trend. This conclusion must be taken with caution as the variation in structural parameters and magnetic coupling values takes place in a short-range for all these compounds.

To support the above conclusion we have performed DFT calculations (see Supporting Information) on the model compound given in Figure 13, in which the C_{phenyl}−O bond

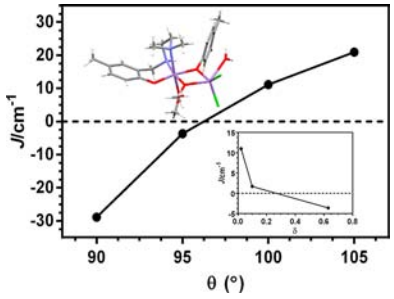

Figure 13. Calculated J values vs the Mn^{2+}−O−Mn^{3+} angle (θ) and calculated J values vs δ (inset) for the model compound indicated in the inset (top left).

involving the methoxy group coordinated to the Mn^{2+} ion and linked to the phenyl ring has been broken and the methoxy group has been replaced by a coordinated water molecule. Moreover, the Mn^{2+}−O and the Mn^{3+}−O bonds in the $Mn^{II}(O)_2Mn^{III}$ bridging fragment have been set to the values Mn(III)−O = 1.917 Å and Mn(II)−O = 2.115 Å. In these calculations, the $Mn^{II}(O)_2Mn^{III}$ bridging fragment was kept with the same angle as in complex **1** and the θ angle varied in the 90−105° range. In all cases, the phenyl ring was turned away from the $Mn^{II}(O)_2Mn^{III}$ bridging plane by 70° to avoid steric hindrance with neighboring parts of the molecule. The DFT results (see Figure 13) clearly show that a relationship exists between J and θ, so that for angles larger than ∼97° (the crossover point below which the magnetic interaction changes from ferromagnetic to antiferromagnetic) the magnetic exchange interaction is ferromagnetic in nature and its magnitude increases when θ increases reaching a value of +20.9 cm^{-1} at 105°. It should be pointed out that the imposed geometrical changes in the model lead to calculated J values that are of the same order of magnitude but higher than the experimental and calculated values for compounds **1**−**6**. To know how the distortion of the SP geometry toward the TBPY-5 geometry of the Mn^{2+} coordination polyhedron affects the J values we have carried out calculations on the model compound for θ = 100° by gradually changing the δ parameter[29] for the Mn^{2+} coordination polyhedron from δ = 0 (ideal SPY-5) to δ = 0.63 (geometry closer to TBPY-5). The three model compounds with different δ values are given in Figure S11. The DFT results (Figure 13, inset) clearly show that the J values are less positive (the F interaction decreases) when δ increases and becomes negative (AF interaction) for δ values above ∼0.20. These theoretical results are in full agreement with the conclusions drawn from the experimental results for compounds **1**−**6**.

The magnetic data for compound **9** were analyzed with the following isotropic Hamiltonian for an isosceles trinuclear triangular system

$$\mathbf{H} = -J_{12}(\mathbf{S}_{Mn1}\mathbf{S}_{Mn2} + \mathbf{S}_{Mn2}\mathbf{S}_{Mn3}) - J_{23}(\mathbf{S}_{Mn1}\mathbf{S}_{Mn1})$$

The fit of the experimental susceptibility data with the above Hamiltonian using the full matrix diagonalization MAGPACK program[44] afforded the following set of parameters: J_{12} = +0.04(7) cm^{-1}, J_{23} = −5.3(1), g = 2.11(1). It should be noted that in this case, with a dominant antiferromagnetic interaction, the influence of local anisotropy on the magnetic properties is very difficult to be evidenced from the magnetic susceptibility data. This is the reason why we have not considered the local anisotropy in the Hamiltonian used for analyzing the magnetic data of **9**. The interaction between the Mn^{II} and Mn^{III} ions through the phenoxo/alkoxo bridging groups is very weak compared to that found in complexes **1**−**6**, which can be due to the shift of the central Mn^{II} atom with respect to the plane containing the four oxygen bridging atoms. This distortion would reduce the more significant ferromagnetic contribution to the magnetic coupling ($dxy \leftrightarrow dx^2-y^2$).

The field dependence of the magnetization matches well with the Brillouin function for an S = 5/2 ground state with g = 2.11, which would appear as a consequence of the stronger antiferromagnetic interaction through the chloride bridge as compared with that mediated by the alkoxo/phenoxo pathway (Figure 14). The fact that the magnetization is not fully

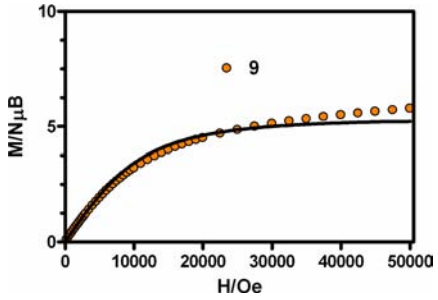

Figure 14. M vs H plot for complex **9**. The solid line corresponds to the Brillouin function for S = 5/2.

saturated at high field may be due to the presence of a significant magnetic anisotropy and/or more likely the presence of low-lying excited states that are partially (thermally and field-induced) populated.

The spin density distributions for the decaplet ground state in **1**−**6** and the sextuplet ground state in **9** (the spin density of **2**, **4**, **8**, and **9** are given as examples in Figures S12−S15) confirm the predominance of the delocalization mechanism through the σ type exchange pathways involving the magnetic orbitals of the Mn^{2+} and Mn^{3+} atoms and the p orbitals of the phenoxo/alkoxo bridging groups (and the chloride bridging group in the case of **9**). It should be noted that there indeed exists spin density on the two semicoordinated methoxo groups in compound **9**, with long Mn−O distances of 2.891 Å and 2.872 Å. A similar but lower spin density is delocalized on the methoxy groups that are located at ∼3 Å in the trinuclear compounds **7** and **8**.

dx.doi.org/10.1021/ic302731z | Inorg. Chem. 2013, 52, 2228−2241

Dynamic ac magnetic measurements were performed to know if complexes **1**−**6** exhibit single-molecule magnet behavior. In spite of the significant anisotropy and $S = 9/2$ ground state for these compounds, they do not show any maximum in out-of-phase susceptibility signals (χ_M'') above 2 K, even in the presence of an small dc applied field. Hence, these complexes do not exhibit slow relaxation of the magnetization and, therefore, SMM behavior.

In this study we have prepared several novel mixed-valence di- and trinuclear manganese(II,III) complexes which hold interesting magnetic properties. In all dinuclear complexes the exchange interaction between Mn^{3+} and Mn^{2+} ions is proven to be ferromagnetic. The prepared complexes can be further modified to produce new complexes with higher nuclearity and/or different bridging groups and diverse magnetic behavior depending on the structural parameters of the bridging network. The analysis of the magnetostructural data for the complexes reported in this paper and other closely related diphenoxo, phenoxo/alkoxo, and dialkoxo doubly bridged dinuclear and trinuclear $Mn^{II}Mn^{III}$ mixed valence complexes seems to indicate that, even though the J values are not very sensible to the Mn^{2+}−O−Mn^{3+} angle (θ), for $\theta > \sim 100°$ ferromagnetic interactions increase when θ increases and the distortion of the Mn^{2+} polyhedron from ideal square pyramidal toward trigonal bipyramidal geometry decreases. These magnetostructural correlations have been supported by DFT calculations on model compounds. Further work is in progress to use the obtained $Mn^{II}Mn^{III}$ mixed valence complexes as tunable building blocks in the difficult task of synthesizing single molecule magnets and other magnetic materials.

■ ASSOCIATED CONTENT

Supporting Information

X-ray crystallographic data for all complexes in CIF format (CDCC 911571−911580), summary of the crystallographic data and selected geometrical parameters for **7**−**9**. Spectroscopic data for complexes **1**−**6** and **9**, ^{1}H NMR spectra and elemental analysis results for ligands are included. This material is available free of charge via the Internet at http://pubs.acs.org.

■ AUTHOR INFORMATION

Corresponding Author

*E-mail: ecolacio@ugr.es (E.C.), resillan@jyu.fi (R.S.).

Notes

The authors declare no competing financial interest.

■ ACKNOWLEDGMENTS

We are grateful to Inorganic Materials Chemistry Graduate Program for financing the project and to Elina Hautakangas for performing the elemental analysis. E.C. and A.J.M. thanks to the Ministerio de Educación Cultura y Deporte (Spain) (Projects CTQ-2008-02269/BQU and CTQ2011-24478), the Junta de Andalucía (FQM-195) and the Universidad de Granada for financial support. We would like to thank the Centro de Supercomputación de la Universidad de Granada for computational resources. We would like also to thank Victor K. Abdelkader, University of Granada, for deconvoluting the XPS spectra. F.L. thanks to the MICINN (Spain) (Project CTQ2010-15364), the University of Valencia (Project UV-INVAE11- 38904) and the Generalitat Valenciana (Spain) (Projects PROMETEO/2009/108, GV/2012/051 and ISIC/2012/002) for financial support.

■ REFERENCES

(1) Dismukes, G. C. *Chem. Rev.* **1996**, *96*, 2909.
(2) Kono, Y.; Fridovich, I. *J. Biol. Chem.* **1983**, *258*, 13646.
(3) Barynin, V. V.; Whittaker, M. M.; Antonyuk, S. V.; Lamzin, S. V.; Harrison, P. M.; Artymiuk, A. J.; Whittaker. *J. Mol. Struct.* **2001**, *9*, 725.
(4) Reczkowski, R. S.; Ash, D. E. *J. Am. Chem. Soc.* **1992**, *114*, 10992.
(5) Cammack, R.; Chapman, A.; Lu, W.-P.; Karagouni, A.; Kelly, D. P. *FEBS Lett.* **1989**, *253* (1−2), 239.
(6) Carrel, H. L.; GLusker, J. P.; Burger, V.; Manfre, F.; Tritsch, D.; Biellmann, J.-F. *Proc. Natl. Acad. Sci* **1989**, *86*, 4440.
(7) Whitlow, M.; Howard, A. J; Finzel, B. C.; Poulos, T. L.; Winborne, E.; Gilliland, G. L. *Proteins* **1991**, *9*, 153.
(8) Collyer, C. A.; Henrick, K.; Blow, D. M. *J. Mol. Biol.* **1990**, *212*, 211.
(9) (a) Cox, N.; Ogata, H.; Stolle, P.; Reijerse, E.; Auling, G.; Lubitz, W. *J. Am. Chem. Soc.* **2010**, *132*, 11197. (b) Cotruvo, J. A.; Stubbe, J. *Biochemistry* **2010**, *49*, 1297.
(10) Dismukes, G. C.; Siderer, Y. *Proc. Natl. Acad. Sci. U.S.A.* **1981**, *78* (1), 274.
(11) Sessoli, R.; Gatteschi, D.; Caneschi, A.; Novak, M. A. *Nature* **1993**, *365*, 141.
(12) For some recent reviews see: (a) Gatteschi, D.; Sessoli, R. *Angew. Chem., Int. Ed.* **2003**, *42*, 268. (b) Christou, G. *Polyhedron* **2005**, *24*, 2065. (c) Gatteschi, D.; Sessoli, R.; Villain, J. *Molecular Nanomagnets*; Oxford University Press: Oxford, UK, 2006. (d) Aromí, G.; Brechin, E. K. *Struct. Bonding (Berlin)* **2006**, *122*, 1. (e) Rebilly, J.-N.; Mallah, T. *Struct. Bonding (Berlin)* **2006**, *122*, 103. (f) Cornia, A.; Costantino, A. F.; Zobbi, L.; Caneschi, A.; Gatteschi, D.; Mannini, M.; Sessoli, R. *Struct. Bonding (Berlin)* **2006**, *122*, 133. (g) Milios, C. J.; Piligkos, S.; Brechin, E. K. *Dalton Trans.* **2008**, 1809. (h) Bagai, R.; Christou, G. *Chem. Soc. Rev.* **2009**, *38*, 1011. (i) Sessoli, R.; Powell, A. K. *Coord. Chem. Rev.* **2009**, *253*, 2328. (j) Andruh, M.; Costes, J. P.; Diaz, C.; Gao, S. *Inorg. Chem.* **2009**, *48*, 3342 (Forum Article). (k) Molecular Magnets themed issue: Brechin, E. K. Ed.; *Dalton Trans.* **2010**. (l) Bagai, R.; Christou, G. *Chem. Soc. Rev.* **2009**, *38*, 1011.
(13) (a) Wernsdorfer, W.; Sessoli, R. *Science* **1999**, *284*, 133. (b) Leuenberger, M. N.; Loss, D. *Nature* **2001**, *410*, 789. (c) Meier, F.; Loss, D. *Physica B* **2003**, *329*, 1140.
(14) Winpenny, R. E. P. *J. Chem. Soc., Dalton Trans.* **2002**, 1.
(15) Mandal, S.; Rosair, G.; Ribas, J.; Bandyopadhyay, D. *Inorg. Chim. Acta* **2009**, *362*, 2200.
(16) Glaser, T. *Chem. Commun.* **2011**, *47*, 116.
(17) Otwinowski, Z.; Minor, W. In *Methods in Enzymology: Part A*; Carter, C. W., Sweet, R. M., Eds.; Academic Press: New York, 1997; Vol. *276*, pp 307−326.
(18) Sheldrick, G. M. *SADABS*; University of Göttingen: Germany, 2002.
(19) *CrysAlisPro*; Agilent Technologies Ltd: Yarnton, England, 2011.
(20) Sheldrick, G. M. *Acta Crystallogr., Sect. A* **2008**, *64*, 112.
(21) Altomare, A.; Burla, M. C.; Camalli, M.; Cascarano, G. L.; Giacovazzo, C.; Guagliardi, A.; Moliterni, A. G. G.; Polidori, G.; Spagna, R. *J. Appl. Crystallogr.* **1999**, *32*, 115.
(22) DIAMOND, *J. Appl. Crystallogr.***1999**, *32*, 1028.
(23) Riisiö, A.; Wichmann, O.; Sillanpää, R. *Lett. Org. Chem.* **2010**, *7*, 298.
(24) (a) Hirotsu, M.; Kojima, M.; Mori, W.; Yoshikawa. *Bull. Chem. Soc. Jpn.* **1998**, *71*, 2873. (b) Hirotsu, M.; Kojima, M.; Yoshikawa, Y. *Bull. Chem. Soc. Jpn.* **1997**, *70*, 649. (c) Schmitt, H.; Lomoth, R.; Magnuson, A.; Park, J.; Fryxelius, J.; Kritikos, M.; Mårtensson, J.; Hammarström, L.; Sun, L.; Åkermark, B. *Chem.—Eur. J.* **2002**, *8*, 3757. (d) Anderlund, M. F.; Zheng, J.; Ghiladi, M.; Kritikos, M.; Riviere, E.; Sun, L.; Girerd, J.-J.; Akermark, B. *Inorg. Chem. Commun.* **2006**, *9*, 1195.
(25) Gómez-Alcántara, M. M.; Aranda, M. A. G.; Olivera-Pastor, P.; Beran, P.; García-Muñoz, J. L.; Cabeza, A. *Dalton Trans.* **2006**, 577.
(26) Llunell, M.; Casanova, D.; Cirera, J.; Bofill, J. M.; Alemany, P.; Alvarez, S.; Pinsky, M.; Avnir, D. *SHAPE* v1.1b; University of Barcelona: Barcelona, 2005.

(27) (a) Taylor, R.; Kennard, O. *J. Am. Chem. Soc.* **1982**, *104*, 5063. (b) Desiraju, G. R. *Acc. Chem. Res.* **1991**, *24*, 290. (c) Steiner, T. *New J. Chem.* **1998**, 1099.
(28) Kahn, O. *Molecular Magnetism*; VCH: Weinheim, Germany, 1993.
(29) Addison, A. W.; Rao, T. N.; Reedijk, J.; Rijn, J.; Verschoor, G. C. *J. Chem. Soc., Dalton Trans.* **1984**, 1349.
(30) (a) Goodenough, J. B. *Phys. Rev.* **1955**, *100*, 564. (b) J. Kanamori, J. *Phys. Chem. Solids* **1959**, *10*, 87.
(31) Liu, H.; Tian, J.; Kou, Y.; Zhang, J.; Feng, L.; Li, D.; Gu, W.; Liu, X.; Liao, D.; Cheng, P.; Ribas, J.; Yan, S. *Dalton Trans.* **2009**, 10511.
(32) Bashkin, J. S.; Schake, A. R.; Vincent, J. B.; Chang, H.-R.; Li, Q.; Huffman, J. C.; Christou, G.; Hendrickson, D. N. *J. Chem. Soc. Chem. Commum.* **1988**, 700.
(33) Gou, S.; Zeng, Q.; Yu, Z.; Qian, M.; Zhu, J.; Duan, C.; You, X. *Inorg. Chim. Acta* **2000**, 175.
(34) Gelasco, A.; Kirk, M. L.; Kampf, J. W.; Pecoraro, V. L. *Inorg. Chem.* **1997**, *36*, 1829.
(35) (a) Bossek, U.; Hummel, H.; Weyhermüuller, T.; Wieghardt, K.; Russell, S.; van der Wolf, L.; Kolb, U. *Angew. Chem.* **1996**, *108*, 1653. (b) Cox, N.; Ames, W.; Epel, B.; Kulik, L. V.; Rapatskiy, L.; Neese, F.; Messinger, J.; Wieghardt, K.; Lubitz, W. *Inorg. Chem.* **2011**, *50*, 8238.
(36) Diril, H.; Chang, H.-R.; Zhang, X.; Larsen, S. K.; Potenza, J. A.; Pierpont, C. G.; Schugar, H. J.; Isied, S. S.; Hendrickson, D. N. *J. Am. Chem. Soc.* **1987**, *109*, 6207.
(37) Chang, H.-R.; Diril, H.; Nilges, M. J.; Zhang, X.; Potenza, J. A.; Schugar, H. J.; Hendrickson, D. N.; Isied, S. S. *J. Am. Chem. Soc.* **1988**, *110*, 625.
(38) Prescimone, A.; Wolowska, J.; Rajaraman, G.; Parsons, S.; Wernsdorfer, W.; Murugesu, M.; Christou, G.; Piligkos, S.; McInnes, E. J. L.; Brechin, E. K. *Dalton Trans.* **2007**, 5282.
(39) Yoshino, A.; Miyagi, T.; Asato, E.; Mikuriya, M.; Sakata, Y.; Sugiura, K.; Iwasaki, K.; Hino, S. *Chem. Commun.* **2000**, 1475.
(40) Hirotsu, M.; Aoyagi, M.; Kojima, M.; Mori, W.; Yoshikawa, Y. *Bull. Chem. Soc. Jpn.* **2002**, *75*, 259.
(41) Mandal, D.; Chatterjee, P. B.; Bhattacharya, S.; Choi, K.-Y.; Clérac, R.; Chaudhury, M. *Inorg. Chem.* **2009**, *48*, 1826.
(42) Hirotsu, M.; Kojima, M.; Yoshikawa, Y. *Bull. Chem. Soc. Jpn.* **1997**, *70*, 649.
(43) (a) Zener, C. *Phys. Rev.* **1951**, *82*, 403. (b) Girerd, J.-J. *J. Chem. Phys.* **1983**, *79*, 1766.
(44) (a) Borrás-Almenar, J. J.; Clemente, J.; Coronado, E.; Tsukerblat, B. S. *Inorg. Chem.* **1999**, *38*, 6081. (b) Borrás-Almenar, J. J.; Clemente, J.; Coronado, E.; Tsukerblat, B. S. *J. Comput. Chem.* **2001**, *22*, 985.